Integrated Nonmagnetic Optical Isolators Based on Photonic Transitions*

Zongfu Yu and Shanhui Fan, *Senior Member, IEEE*

(Invited Paper)

***Abstract*—Based on the effects of photonic transitions, here we show that a linear, broadband, and nonreciprocal isolator can be accomplished by spatial–temporal refractive index modulations that simultaneously impart frequency and wave vector shifts during the photonic transition process. This paper demonstrates that on-chip isolation can be accomplished with dynamic photonic structures in standard material systems that are widely used for integrated optoelectronic applications.**

***Index Terms*—Integrated optical isolator, nonreciprocal optics, photonic transition, refractive index modulation.**

I. Introduction

ACHIEVING on-chip optical signal isolation is a fundamental difficulty in integrated photonics [1]. The need to overcome this difficulty, moreover, is becoming increasingly urgent, especially with the emergence of silicon nanophotonics [2]–[4], which promises to create on-chip optical systems at an unprecedented scale of integration.

To create complete optical signal isolation requires simultaneous breaking of both the time reversal and the spatial inversion symmetry. In bulk optics, this is achieved using materials exhibiting magneto-optical effects [5]–[10]. However, on-chip integration of magneto-optical materials, especially in silicon in a CMOS-compatible fashion, remains a challenge since magneto-optical materials are not the standard material system used in the CMOS process. Alternatively, optical isolation has also been observed using nonlinear optical processes [11], [12], or in electro-optic modulators [13]. In either case, however, optical isolation occurs only at specific power ranges, or with either associated modulation sidebands or substantial intrinsic loss [13]. In addition, there have been works aiming to achieve partial optical isolation in reciprocal structures that have no inversion symmetry (e.g., chiral structures) [14]. In these systems, the apparent isolation occurs by restricting the allowed photon states in the backward direction, and would not work for arbitrary backward incoming states. None of the aforementioned nonmagnetic schemes can provide complete optical isolation.

In this paper, we review and expand our recent works [15], [16] on creating complete and linear optical isolation using dynamic photonic structures, where the refractive index of the structure is modulated as a function of time and space. In these works, the temporal profile of the modulation is chosen to break the time-reversal symmetry, while the spatial profile of the modulation is chosen to break the spatial inversion and the mirror symmetry. While the existence of nonreciprocity in electro-optic and acoustic modulation has long been noted before [17], the possibility of creating complete optical isolation based on such modulation was not explicitly studied and is the subject of this paper.

The underlying physical mechanism of our isolator structures relies upon the photonic transition effect as induced by refractive index modulation. It was shown theoretically [18] that when photonic structures are subjected to temporal refractive index modulation, photon states can go through interband transitions, in a direct analogy to electronic transitions in semiconductors. Such photonic transitions have been recently demonstrated experimentally in silicon microring resonators [19]. In our recent work [15], [16], we showed that with appropriately designed band structure, and by choosing a spatially and temporally varying modulation format that simultaneously imparts frequency and momentum shifts of photon states during the transition process, the transmission behavior of a photonic structure can become nonreciprocal. As seen in the finite-difference time-domain simulations [20], when a silicon waveguide is under a modulation, the details of which will be described in the following sections of the paper, light of frequency ω_1 in forward direction is converted to a higher frequency mode ω_2 by the modulation [see Fig. 1(a)]. At the same time, light of frequencies ω_1 or ω_2 in the backward direction are not affected by the modulation [Fig. 1(b) and (c)]. Combined with an absorption filter centered at ω_2, this structure can absorb all light incident from one direction at ω_1, while passing those in the opposite direction, and thus, creates a complete isolator behavior. It was also shown that the finite-difference time-domain simulations can also be well reproduced by coupled mode theory [15].

In this paper, we will use the coupled mode theory to discuss the performance and design considerations for dynamic isolator schemes. The paper is organized as follows. In Section II, we review the physical mechanism of using interband transition for optical isolation. In Section III, we analyze the performance of the isolator including the bandwidth and device size. Finally, in

*This paper should have appeared in *Selected Topics in Quantum Electronics*, Special Issue on Silicon Photonics, January/February 2010, Vol. 16, No. 1. It was inadvertently omitted from the issue.

Manuscript received May 5, 2009; revised June 7, 2009. First published November 6, 2009; current version published April 7, 2010. This work was supported by the National Science Foundation under Grant ECS-0622212.

Z. Yu is with the Department of Applied Physics, Stanford University, Stanford, CA 94305 USA (e-mail: zfyu@stanford.edu).

S. Fan is with the Department of Electrical Engineering, Stanford University, Stanford, CA 94305 USA (e-mail: shanhui@stanford.edu).

Color versions of one or more of the figures in this paper are available online at http://ieeexplore.ieee.org.

Digital Object Identifier 10.1109/JSTQE.2009.2026914

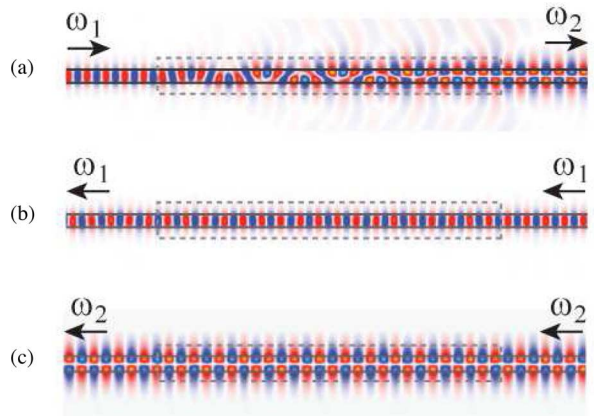

Fig. 1. Finite-difference time-domain simulation of an isolator based on photonic transitions. The box indicates the regions where the refractive index is modulated. Blue/red show the amplitude of electric fields. Arrows indicate propagation directions.

Section IV, we demonstrate two alternative isolator structures to suit different performance requirements.

II. Theory of the Nonreciprocal Mode Conversion in Interband Photonic Transitions

We start by considering the photon transition process in a silicon waveguide. The waveguide (assumed to be 2-D for simplicity) is represented by a dielectric distribution $\varepsilon_s(x)$, which is time-independent and uniform along the z-direction [Fig. 2(b)]. Such a waveguide possesses a band structure, as shown in Fig. 2(a), with symmetric and antisymmetric modes located in the first and second band, respectively. An interband transition between two modes with frequencies and wave vectors $(\omega_1, k_1), (\omega_2, k_2)$ located in these two bands, can be induced by modulating the waveguide with an additional dielectric perturbation

$$\varepsilon'(x,z,t) = \delta(x)\cos(\Omega t - qz) \tag{1}$$

where $\delta(x)$ is the modulation amplitude distribution along the direction transverse to the waveguide and $\Omega = \omega_2 - \omega_1$ is the modulation frequency. Fig. 2(c) shows the profile of the modulation. Such a transition with $k_1 \neq k_2$ is referred to as an indirect photonic transition, in analogy with indirect electronic transitions in semiconductors.

We assume that the wave vector q approximately satisfies the phase matching condition, i.e., $\Delta k = k_2 - k_1 - q \approx 0$. In the modulated waveguide, the electric field becomes

$$E(x,z,t) = a_1(z)E_1(x)e^{i(-k_1 z+\omega_1 t)} + a_2(z)E_2(x)e^{i(-k_2 z+\omega_2 t)} \tag{2}$$

where $E_{1,2}(x)$ are the modal profiles, satisfying the orthogonal condition (For simplicity, we have assumed the TE modes where the electric field has components only along the y-direction.)

$$\frac{v_{gi}}{2\omega_i}\int_{-\infty}^{\infty}\varepsilon(x)E_i^* E_j = \delta_{ij}. \tag{3}$$

In (3), the normalization is chosen such that $|a_n|^2$ is the photon number flux carried by the nth mode. By substituting (2) into

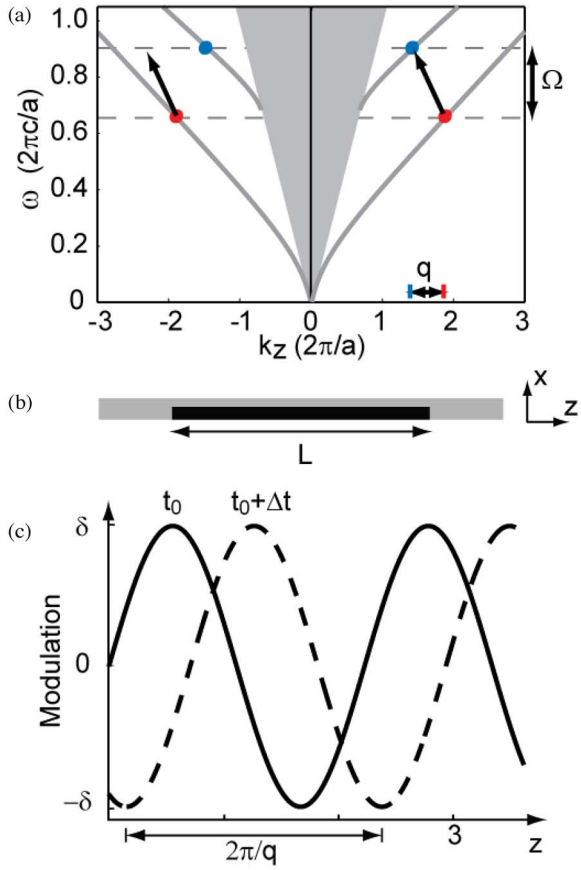

Fig. 2. (a) Band structure of a slab waveguide. (b) Structure of the silicon ($\varepsilon_s = 12.25$) waveguide. Modulation is applied to the dark region. (c) Modulation profile at two sequential time steps.

the Maxwell's equations, and using slowly varying envelope approximation, we can derive the coupled mode equation

$$\frac{d}{dz}\begin{pmatrix} a_1 \\ a_2 \end{pmatrix} = \begin{pmatrix} 0 & i\frac{\pi}{2l_c}\exp(-i\Delta k z) \\ i\frac{\pi}{2l_c}\exp(i\Delta k z) & 0 \end{pmatrix}\begin{pmatrix} a_1 \\ a_2 \end{pmatrix} \tag{4}$$

where

$$l_c = \frac{4\pi}{\varepsilon_0\int_{-\infty}^{\infty}\delta(x)E_1(x)E_2(x)dx} \tag{5}$$

is the coherence length. With an initial condition $a_1(0) = 1$ and $a_2(0) = 0$, the solution to (4) is

$$\begin{aligned} a_1(z) &= e^{-iz\Delta k/2}\left[\cos\left(\frac{z}{2l_c}\sqrt{\pi^2 + (l_c\Delta k)^2}\right)\right. \\ &\quad \left. + i\frac{l_c\Delta k}{\sqrt{\pi^2 + (l_c\Delta k)^2}}\sin\left(\frac{z}{2l_c}\sqrt{\pi^2 + (l_c\Delta k)^2}\right)\right] \\ a_2(z) &= ie^{iz\Delta k/2}\frac{\pi}{\sqrt{\pi^2 + (l_c\Delta k)^2}}\sin\left(\frac{z}{2l_c}\sqrt{\pi^2 + (l_c\Delta k)^2}\right]. \end{aligned} \tag{6}$$

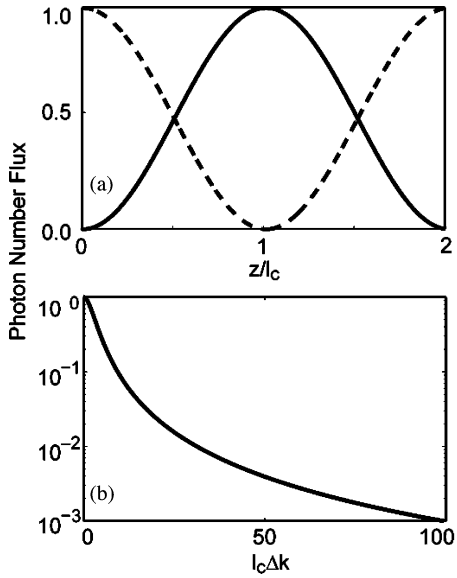

Fig. 3. (a) Spatial evolution of the photon number flux of two modes (dashed line: mode 1 and solid line: mode 2) when a phase matching modulation is applied to the waveguide. (b) Maximum photon flux in mode 2 for nonzero phase mismatch.

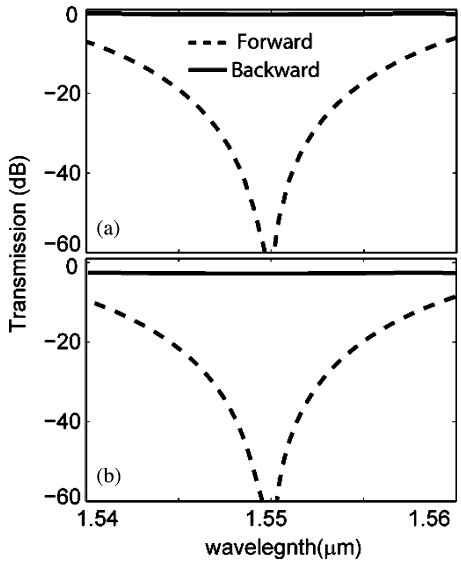

Fig. 4. Forward and backward transmission spectra without (a) and with (b) modulation loss.

In the case of perfect phase matching, i.e., $\Delta k = 0$, a photon initially in mode 1 will make a complete transition to mode 2 after propagating over a distance of coherence length l_c [see Fig. 3(a)]. In contrast, in the case of strong phase mismatch, i.e., $l_c \Delta k \gg 1$, the transition amplitude is negligible [Fig. 3(b)].

The system described earlier exhibits strong nonreciprocal behavior: the modulation in (1) does not phase match the mode at $(\omega_1, -k_1)$ with any other mode of the system [Fig. 2(a)]. Thus, while the mode at (ω_1, k_1) undergoes a complete photonic transition, its time-reversed counterpart at $(\omega_1, -k_1)$ is not affected at all. Such nonreciprocity arises from the breaking of *both* time reversal and spatial inversion symmetries in the dynamics. The modulation in (1) is *not* invariant with either $t \to -t$ or $z \to -z$.

As a specific example, we consider a silicon $(\varepsilon = 12.25)$ waveguide of 0.27 μm wide, chosen such that the first and second bands of the waveguide have the same group velocity around wavelength 1.55 μm (or a frequency of 193 THz). The modulation has a strength $\delta_{\max}/\varepsilon_s = 5 \times 10^{-4}$, a frequency $\Omega/2\pi = 20$ GHz, and a spatial period $2\pi/|q| = 0.886$ μm (all these parameters should be achievable in experiments). The modulation is applied to half of the waveguide width so that the even and odd modes can couple efficiently. The modulation length L is chosen as the coherence length $l_{c0} = 2.19\,\mathrm{mm}$ [Fig. 2(b)] for operation frequency ω_0 at 1.55 μm wavelength. Fig. 4(a) shows the transmission for forward and backward directions. The bandwidth is 5 nm with contrast ratio above 30 dB.

For the loss induced by refractive index modulation schemes, e.g., carrier injection modulation, the contrast ratio remains approximately the same as the lossless case, since the modulation loss applies to transmission in both directions. Thus, the isolation effect is not affected. As an example, the modulation strength used here $\delta/\varepsilon_s = 5 \times 10^{-4}$ results in a propagating loss of $1.5\,\mathrm{cm}^{-1}$ in silicon [21]. This causes an insertion loss of about -3.5 dB while the bandwidth remains approximately unchanged [Fig. 4(b)].

In general, similar nonreciprocal effects can also be observed in intraband transitions. However, since typically $\Omega \ll \omega_1$, and the dispersion relation of a single band can typically be approximated as linear in the vicinity of ω_1, a cascaded process [19], which generates frequencies at $\omega_1 + n\Omega$ with $n > 1$, is unavoidable, and it complicates the device performance. In contrast, the interband transition here eliminates the cascaded processes.

We would like to emphasize that the modulation frequency can be far smaller than the bandwidth of the signal. This is, in fact, one of the key advantages of using interband transition. The transition occurs from a fundamental even mode to a second-order odd mode. The generated odd mode can be removed with the use of mode filters that operate based on modal profiles. Examples of such mode filters can be found in [22] and [23]. It is important to point out that such mode filters are purely passive and reciprocal, and can be readily implemented on chip in a very compact fashion. Moreover, in Section IV, we will discuss the implementation of an isolator without the use of modal filters.

In order to achieve the required modulation profile, particularly the spatial periodic modulation, one can use three uniformly modulated regions for each spatial period. Each region is modulated by an oscillating signal of frequency Ω. In addition, the neighboring region has a phase difference of $2\pi/3$. Such scheme provides a simplified implementation of the modulation profile in (1) with negligible performance difference, as verified by coupled mode calculation.

III. Device Performance

The isolation effect and results of the coupled mode theory have been verified by numerical simulation using the finite-difference time-domain method [15], which solves Maxwell

equation without any approximation. Based on the coupled mode theory, we analyze in detail various aspects regarding the performance of the proposed isolator, including, in particular, its operational bandwidth and device size, later in this section.

A. Bandwidth

The dynamic isolator structure creates contrast between forward and backward propagations by achieving complete frequency conversion only in the forward direction. As discussed earlier, the modulation is chosen such that it induces a phase-matched transition from an even mode at the frequency ω_0 to an odd mode at the frequency of $\omega_0 + \Omega$. The length of the waveguide is chosen to be the coherence length $l_c(\omega_0)$ for this transition, such that complete conversion occurs at this frequency ω_0 for the incident light. In order to achieve a broadband operation, one would need to achieve near-complete conversion for all incident light having frequencies ω in the vicinity of ω_0 as well. From (6), broadband operation, therefore, requires that

$$\begin{aligned} &\Delta k(\omega) = 0 \\ &l_c(\omega) = L = l_c(\omega_0). \end{aligned} \tag{7}$$

The first condition in (7) implies that the phase matching condition needs to be achieved over a broad range of frequencies, and the second condition implies that the coherence length should not vary as a function of frequency. Deviations from these conditions result in a finite operational bandwidth.

We consider the phase matching condition first. In the vicinity of the design frequency ω_0, the wave vector mismatch can be approximated by

$$\Delta k = k_1(\omega) - k_2(\omega+\Omega) - q \approx \left(\frac{1}{v_{g1}(\omega)} - \frac{1}{v_{g2}(\omega+\Omega)}\right)\Delta\omega + \frac{1}{2}\left(\frac{d^2k_1(\omega)}{d\omega^2} - \frac{d^2k_2(\omega+\Omega)}{d\omega^2}\right)\Delta\omega^2\Big|_{\omega=\omega_0}.$$

Thus, to minimize the phase mismatch, it is necessary, first of all, that the two bands have the same group velocities, i.e., the two bands are parallel to each other. Moreover, it is desirable that the group velocity dispersion of the two bands matches with one another. As a quantitative estimate, assuming that $l_c(\omega) \approx L$ for all frequencies, Fig. 5(a) shows the forward transmission as a function of $L\Delta k$. For a transmission below -30 dB, this requires a phase mismatch of $L\Delta k < 0.1$. As a concrete example for comparison purposes, Fig. 6(a) shows the phase mismatch $L\Delta k$ as a function of wavelength for the structure simulated in Fig. 4. Notice that $L\Delta k < 0.1$ over a bandwidth of 5 nm due to the mismatch of group velocity dispersion in the two guided mode bands.

For the second condition in (7), we note that in most waveguide structures, since the coherence length is determined by the modal profile, it generally varies slowly as a function of frequency. For example, for a waveguide with parameters chosen in Section II, the coherence length varies less than 2% over 20 nm bandwidth around 1.55 μm wavelength [Fig. 6(b)]. As a simple estimate of how coherence length variation impacts device performance, assuming $\Delta k(\omega) = 0$ over a broad frequency range, we calculate the forward transmission as a function of coherence length given the modulation length $L = l_c(\omega = \omega_0)$ [Fig. 5(b)]. For 2% variation of the coherence length, the forward transmission remains below -30 dB. Comparing Fig. 6(a) and (b), therefore, we conclude that for the structure simulated in Fig. 4, the 5 nm bandwidth is primarily limited by group velocity dispersion of the two waveguide bands. Since the structure used in Fig. 4 is rather simple, we believe that substantial further enhancement of operating bandwidth is achievable by optimization of waveguide geometry.

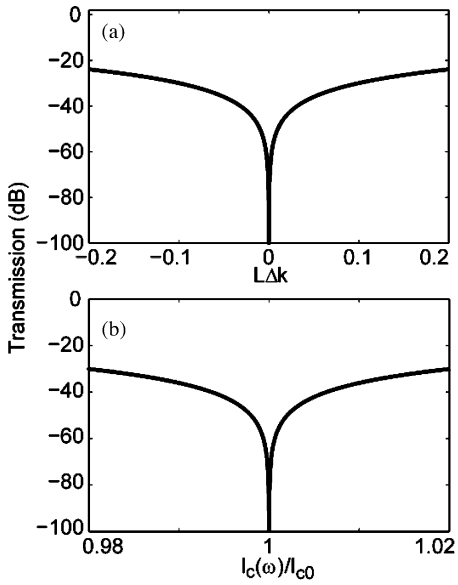

Fig. 5. (a) Forward transmission as a function of phase mismatch. (b) Coherence length variation.

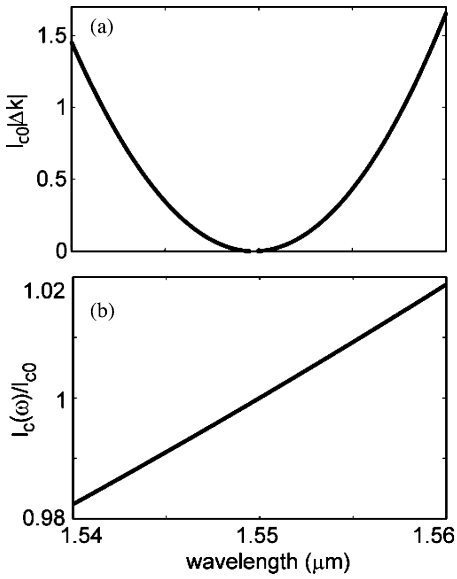

Fig. 6. (a) Phase mismatch and (b) coherence length as a function of wavelength for the device simulated in Fig. 4.

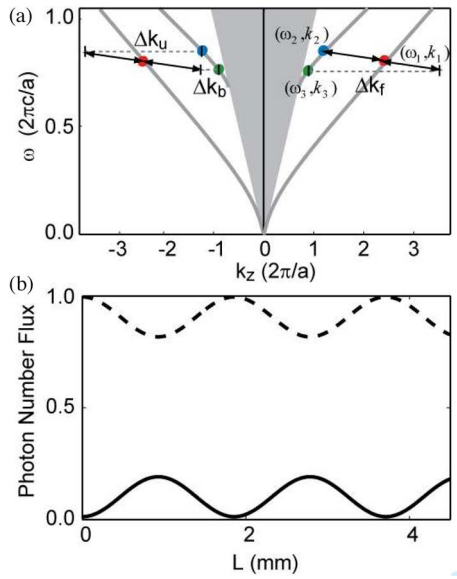

Fig. 7. (a) Transition diagram for low-frequency modulation. (b) Spatial evolution of photon flux in the backward direction for an even mode at 1.55 μm wavelength (dashed line) and an odd mode (solid line) that is 20 GHz lower in frequency. The structure has the same parameters as described in Section II.

B. Device Size

The size of the isolator is determined by the coherence length l_c. Starting from (5), and taking into account the normalization of E field [see (3)], the coherence length can be written as

$$l_c = \frac{4\pi}{\varepsilon_0 \int_{-\infty}^{\infty} \delta(x) E_1(x) E_2(x)\, dx} = \frac{2\pi}{\gamma}\sqrt{\frac{v_{g1} v_{g2}}{\omega_1 \omega_2}} \approx \lambda_0 \times \frac{1}{\gamma} \times \frac{v_g}{c} \tag{8}$$

where

$$\gamma = \frac{\int_{-\infty}^{\infty} \delta(x) E_1(x) E_2(x)\, dx}{\sqrt{\int_{-\infty}^{\infty} \varepsilon(x)|E_1|^2 dx \int_{-\infty}^{\infty} \varepsilon(x)|E_2|^2 dx}}$$

characterizes the effect of modulation. In deriving (8), we assume that $\omega_1 \approx \omega_2 \equiv 2\pi c/\lambda_0$, where λ_0 is the wavelength in vacuum, since the modulation frequency is typically far smaller than the optical frequency. Moreover, the two bands are assumed to be parallel to each other, i.e., $v_{g1} \approx v_{g2} \equiv v_g$. Equation (8) indicates that the device size is proportional to the group velocity and is inversely proportional to the modulation strength. For a rough estimate, with a modulation strength $\gamma \sim (\delta/\varepsilon) \sim 10^{-4}$, operating at a wavelength of $\lambda \sim 1.5\ \mu$m and $v_g \approx c/3$, the coherence length $l_c \sim 5$ mm. To reduce the size, one can use stronger modulation strength and/or slow light waveguides.

C. Near-Phase-Matched Transition in the Backward Direction

In general, due to energy conservation constraint, a mode with a frequency of ω_1 can only make a transition to modes at $\omega_1 \pm \Omega$. In our design, the modulation is chosen to create a phase-matched transition in the forward direction. However, for most electro-optic or acoustic–optic modulation schemes, the modulation frequency $\Omega \leq 100$ GHz is much smaller than the optical frequency. Consequently, as can be seen from Fig. 7(a), in the backward direction, the transition to the mode in the second band with a frequency $\omega_3 = \omega_1 - \Omega$ becomes nearly phase-matched. The wave vector mismatch of this transition is

$$\Delta k_b = -k_2(\omega_1 - \Omega) + k_1(\omega_1) + q \approx \frac{2\Omega}{v_g}. \tag{9}$$

Such a transition results in loss in the backward direction, and thus, a reduction of contrast between the forward and backward directions.

To calculate such transmission loss in the backward direction, we replace Δk in (6) with Δk_b. In general, in order to suppress such backward transmission loss, one needs to have

$$\Delta k_b L \geq 1. \tag{10}$$

Combining with (8), the condition of (10) is then transformed to

$$\frac{2\lambda_0}{c} \times \frac{\Omega}{\gamma} \geq 1. \tag{11}$$

Remarkably, we note from (11) that for electro-optic or acoustic–optic modulation schemes, the effects of weak refractive index modulation γ and low modulation frequency Ω cancel each other out. The use of weak refractive index modulation results in a long coherence length, which helps in suppressing the transition processes that are not phase-matched. It is precisely such a cancellation that enables the construction of dynamic isolators with practical modulation mechanisms.

For the example shown in Fig. 4, the near-phase-matched transition in the backward direction has a $\Delta k_b = 2\pi/2.06$ mm, and thus, $\Delta k_b L = 6.7$, which results in a loss of -0.22 dB for the backward transmission [Fig. 7(b)].

IV. Design Flexibility

In the previous sections, we have shown that by using interband transition, one can create nonreciprocal mode conversion in a waveguide. Such a waveguide works as an isolator when combined with a modal filter. The performance of such a device can be analyzed and optimized using coupled mode theory. In this section, we present two examples to show that such nonreciprocal photon transition can be exploited in a wide range of structures to form nonreciprocal optical devices that satisfy diverse performance requirements. In the first example, we design a four-port isolator/circulator using nonreciprocal phaseshift in the interband transitions. In the second example, we use a nonreciprocal ring resonator to demonstrate a compact design for optical isolation.

A. Four-Port Circulator

Fig. 8(a) shows the design of a four-port circulator [16]. The structure consists of a Mach–Zehdner interferometer, in which one waveguide arm is subject to the dynamic modulation described previously. In contrast to the design in Section III, however, here the length of the modulation region is chosen to be twice the coherence length $L = 2l_c$. Thus, light passing through the modulated waveguide in the forward direction

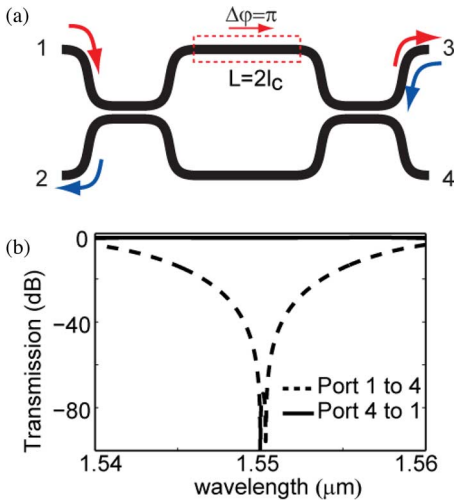

Fig. 8. (a) Schematic and (b) transmission spectrum of a four-port circulator. The dynamic index modulation is applied to the waveguide in the dashed red box.

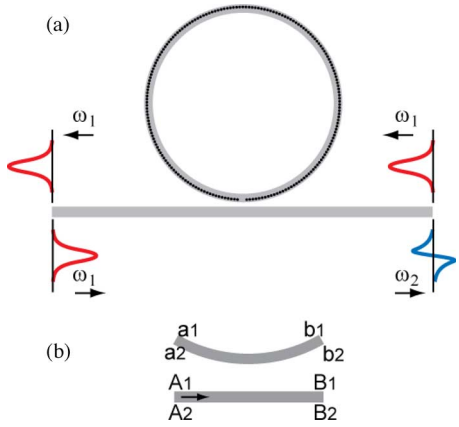

Fig. 9. (a) Schematic of ring resonator designed for nonreciprocal frequency conversion. The dark regions are modulated. (b) Schematic of the modes in the ring waveguide coupling region.

will return to the incident frequency [Fig. 3(a)]. However, such light experiences a nonreciprocal phaseshift due to the photonic transition effect. The use of a Mach–Zehnder interferometer configuration then allows one to construct a circulator. Here, no filter is required, which significantly reduces the device complexity.

For concreteness, we assume that the interferometer has two arms with equal length, and uses two 50/50 waveguide couplers. For such an interferometer, the transmission is described by [24]

$$\begin{pmatrix} b_u \\ b_l \end{pmatrix}_{\mathrm{OUT}} = \frac{1}{2}\begin{pmatrix} 1 & i \\ i & 1 \end{pmatrix}\begin{pmatrix} T\exp(i\varphi_p) & 0 \\ 0 & \exp(i\varphi_p) \end{pmatrix} \times \begin{pmatrix} 1 & i \\ i & 1 \end{pmatrix}\begin{pmatrix} b_u \\ b_l \end{pmatrix}_{\mathrm{IN}}. \quad (12)$$

Here, the subscript "IN" and "OUT" label the input or output, $b_{u/l}$ are the input or output amplitudes in the upper/lower arm, and φ_p is the phase acquired due to propagation in the absence of modulation.

In (12), the transmission coefficient through the upper arm has an additional contribution from the photon transition

$$T = e^{-iz\Delta k/2}\left[\cos\left(\frac{z}{2l_c}\sqrt{\pi^2+(l_c\Delta k)^2}\right) + i\frac{l_c\Delta k}{\sqrt{\pi^2+(l_c\Delta k)^2}}\sin\left(\frac{z}{2l_c}\sqrt{\pi^2+(l_c\Delta k)^2}\right)\right] \quad (13)$$

which influences both the transmission amplitude and the phase as the wave passes through the upper arm. In our design, we assume a phase matching modulation with $\Delta k = 0$ for the forward direction, and use a modulated region with $L = 2l_c$. Equation (13) shows $T = -1$. In contrast, for the light in the backward direction in the upper arm, in general, the phase matching condition is not satisfied. Hence, $T \approx 1$. Thus, in this design, the modulation does not create any frequency conversion. Instead, its sole effect is to induce a nonreciprocal π-phaseshift in the upper arm.

The interferometer in Fig. 8 exploits such nonreciprocal phase to create a circulator. We have used the coupled mode theory developed in Section III to simulate this structure, assuming the same waveguide parameters as in Fig. 4. The results, shown in Fig. 8, indicate that lights injected into port 1 completely output through port 3, while in the time-reversed case, lights injected into port 3 end up in port 2. Therefore, this device has exactly the same response function of a four-port circulator [25]. Unlike conventional design, however, no magnetic components are used inside the structure. Alternatively, the device can also function as a two-port isolator. Fig. 8(b) shows the transmission spectra in both directions between ports 1 and 4: lights incident from port 4 transmit to port 1, while the reverse transmission is completely suppressed. The contrast ratio for the two directions is above 30 dB for a bandwidth of 5 nm [see Fig. 8(b)].

B. Nonreciprocal Ring Resonator

As discussed before, the device size is determined by the coherence length, which, typically, is above millimeters, unless slow light waveguides are used. Substantial reduction of the device footprint can be accomplished using resonator structure at the expense of a smaller operating bandwidth [15]. As an example, we consider a ring resonator [Fig. 9(a)] that supports two anticlockwise rotating resonances, at frequencies ω_1 and ω_2, respectively. Each resonance is further characterized by its wave vectors k_1 and k_2 in the waveguide that forms the ring. These two resonances are coupled by applying a dielectric constant modulation along the ring with a profile $\delta(x)\cos[(\omega_1-\omega_2)t-(k_1-k_2)z]$, where z measures the propagation distance on the circumference of the ring in counterclockwise direction.

To describe the action of this structure, we note that upon completing one round trip, the circulating amplitudes $a_{1,2}$ and $b_{1,2}$ of these two modes [Fig. 9(b)] are related by

$$\begin{pmatrix} a_1 \\ a_2 \end{pmatrix} = \begin{pmatrix} T_{11} & T_{12} \\ T_{21} & T_{22} \end{pmatrix}\begin{pmatrix} b_1 \\ b_2 \end{pmatrix} \quad (14)$$

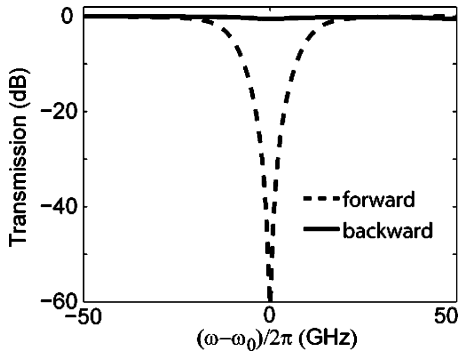

Fig. 10. Transmission spectra of a ring resonator isolator. ω_0 corresponds to 1.55 μm wavelength. The waveguide ring transmit coefficient is assumed to be $r_{1,2} = 0.95$.

where the matrix elements are related to the transition amplitudes for a single round trip, and can be calculated using (4). Each of these modes is also coupled to an external waveguide as described by

$$\begin{pmatrix} b_1 \\ B_1 \\ b_2 \\ B_2 \end{pmatrix} = \begin{pmatrix} r_1 & jt_1 & 0 & 0 \\ jt_1 & r_1 & 0 & 0 \\ 0 & 0 & r_2 & jt_2 \\ 0 & 0 & jt_2 & r_2 \end{pmatrix} \begin{pmatrix} a_1 \\ A_1 \\ a_2 \\ A_2 \end{pmatrix}. \tag{15}$$

The external waveguide is also assumed to support two modes with opposite symmetry at the frequencies ω_1 and ω_2, respectively. Here, the subscripts label the two frequencies, and $A_{1,2}$ and $a_{1,2}$ ($B_{1,2}$ and $b_{1,2}$) are the photon flux amplitudes in the external and ring waveguides before (after) the coupler. The coefficients *r* and *t* are taken to be real [26] and $r_{1,2}^2 + t_{1,2}^2 = 1$.

With incident light in mode 1 (i.e., $A_1 = 1$, $A_2 = 0$) of the external waveguide, combining (14) and (15), we have

$$B_1 = \frac{r_1 - T_{11} - r_1 r_2 T_{22} + r_2 \mathrm{Det}[T]}{1 - r_1 T_{11} - r_2 T_{22} + r_1 r_2 \mathrm{Det}[T]} \tag{16}$$

where Det stands for determinant. Thus, the condition for complete frequency conversion (i.e., $B_1 = 0$) is

$$r_1 - T_{11} - r_1 r_2 T_{22} + r_2 \mathrm{Det}[T] = 0. \tag{17}$$

In the case that ring is lossless, Det[*T*] = 1 and $T_{11} = T_{22} = \cos(\frac{\pi}{2} \ \frac{L}{l_c})$, where l_c is the coherence length and *L* is the circumference of the ring. Complete conversion between the two modes can be achieved when the length of the ring is chosen to be

$$\cos\left(\frac{\pi}{2} \quad \frac{L}{l_c}\right) = \frac{r_1 + r_2}{1 + r_1 r_2}. \tag{18}$$

With $r_{1,2} \to 1$, $L/l_c \to 0$, the device, therefore, can provide complete frequency conversion even when its length is far smaller than the coherence length.

As an example, now we use the same waveguide discussed in Fig. 4 to form a ring with a radius $r = 12.3$ μm. Such a ring supports two resonant modes: a first band resonant mode at 1.55 μm and a second band mode that is 50 GHz higher in frequency. (This is always achievable by fine-tuning the radius and width of the waveguide.) A phase matching modulation is applied to the ring with a coherence length $l_c = 2.37$ mm. At the design wavelength 1.55 μm, the forward transmission is completely suppressed (see Fig. 10). Here, complete isolation is achieved with a device size much smaller than the coherence length.

V. Conclusion

In this paper, we have provided some of the detailed theoretical considerations for the dynamic isolator structures that we have recently proposed. In contrast to previously considered isolators based on material nonlinearity [11], [12], where isolation is only achievable for a range of incident power, the photonic transition effect studied here is *linear* with respect to the incident light: the effect does not depend upon the amplitude and phase of the incident light. Having a linear process is crucial because the device operation needs to be independent of the format, the timing, and the intensity of the pulses used in the system. In conclusion, the structure proposed here shows that on-chip isolation can be accomplished with dynamic modulation in standard material systems that are widely used for integrated optoelectronic applications.

References

[1] M. Soljacic and J. D. Joannopoulos, "Enhancement of nonlinear effects using photonic crystals," *Nat. Mater.*, vol. 3, pp. 211–219, 2004.
[2] L. Pavesi and D. J. Lockwood, *Silicon Photonics*. Berlin, Germany: Springer-Verlag, 2004.
[3] V. R. Almeida, C. A. Barrios, P. R. Panepucci, and M. Lipson, "All-optical control of light on a silicon chip," *Nature*, vol. 431, pp. 1081–1084, 2004.
[4] D. A. B. Miller, "Optical interconnects to silicon," *IEEE J. Sel. Topics Quantum Electron.*, vol. 6, no. 6, pp. 1312–1317, Nov./Dec. 2000.
[5] R. L. Espinola, T. Izuhara, M. C. Tsai, R. M. Osgood, Jr., and H. Dötsch, "Magneto-optical nonreciprocal phase shift in garnet/silicon-on-insulator waveguides," *Opt. Lett.*, vol. 29, pp. 941–943, 2004.
[6] M. Levy, "A nanomagnetic route to bias-magnet-free, on-chip Faraday rotators," *J. Opt. Soc. Amer. B*, vol. 22, pp. 254–260, 2005.
[7] T. R. Zaman, X. Guo, and R. J. Ram, "Faraday rotation in an InP waveguide," *Appl. Phys. Lett.*, vol. 90, pp. 023514-1–023514-3, 2007.
[8] H. Dötsch, N. Bahlmann, O. Zhuromskyy, M. Hammer, L. Wilkens, R. Gerhardt, P. Hertel, and A. Popkov, "Applications of magneto-optical waveguides in integrated optics: Review," *J. Opt. Soc. Amer. B*, vol. 22, pp. 240–253, 2005.
[9] Y. Shoji, T. Mizumoto, H. Yokoi, I. W. Hsieh, and R. M. Osgood, "Magneto-optical isolator with silicon waveguides fabricated by direct bonding," *Appl. Phys. Lett.*, vol. 92, pp. 071117-1–071117-3, 2008.
[10] Y. Shoji and T. Mizumoto, "Ultra-wideband design of waveguide magneto-optical isolator operating in 1.31 μm and 1.55 μm band," *Opt. Exp.*, vol. 15, no. 2, pp. 639–645, 2007.
[11] M. Soljacic, C. Luo, J. D. Joannopoulos, and S. Fan, "Nonlinear photonic microdevices for optical integration," *Opt. Lett.*, vol. 28, pp. 637–639, 2003.
[12] K. Gallo, G. Assanto, K. R. Parameswaran, and M. M. Fejer, "All-optical diode in a periodically poled lithium niobate waveguide," *Appl. Phys. Lett.*, vol. 79, pp. 314–316, 2001.
[13] S. K. Ibrahim, S. Bhandare, D. Sandel, H. Zhang, and R. Noe, "Non-magnetic 30 dB integrated optical isolator in III/V material," *Electron. Lett.*, vol. 40, pp. 1293–1294, 2004.
[14] G. Shvets, "Optical polarizer/isolator based on rectangular waveguide with helical grooves," *Appl. Phys. Lett.*, vol. 89, pp. 141127-1–141127-3, 2006.
[15] Z. Yu and S. Fan, "Complete optical isolation created by indirect interband photonic transitions," *Nat. Photon.*, vol. 3, pp. 91–94, 2009.
[16] Z. Yu and S. Fan, "Optical isolation based on nonreciprocal phase shift induced by interband photonic transitions," *Appl. Phys. Lett.*, vol. 94, pp. 171116-1–171116-3, 2009.

[17] S. Harris and R. Wallace, "Acousto-optic tunable filter," *J. Opt. Soc. Amer.*, vol. 59, pp. 744–747, 1969.
[18] J. N. Winn, S. Fan, J. D. Joannopoulos, and E. P. Ippen, "Interband transitions in photonic crystals," *Phys. Rev. B*, vol. 59, pp. 1551–1554, 1999.
[19] P. Dong, S. F. Preble, J. T. Robinson, S. Manipatruni, and M. Lipson, "Inducing photonic transitions between discrete modes in a silicon optical microcavity," *Phys. Rev. Lett.*, vol. 100, pp. 033904-1–033904-4, 2008.
[20] A. Taflove and S. C. Hagness, *Computational Electrodynamics: The Finite-Difference Time-Domain Method*, 2nd ed. Boston, MA: Artech House, 2000.
[21] R. Soref and B. Bennett, "Electrooptical effects in silicon," *IEEE J. Quantum Electron.*, vol. 23, no. 1, pp. 123–129, Jan. 1987.
[22] Y. Jiao, S. Fan, and D. A. B. Miller, "Demonstrations of systematic photonic crystal design and optimization by low rank adjustment: An extremely compact mode separator," *Opt. Lett.*, vol. 30, pp. 141–143, 2005.
[23] B. T. Lee and S. Y. Shin, "Mode-order converter in a multimode waveguide," *Opt. Lett.*, vol. 28, pp. 1660–1662, 2003.
[24] B. E. A. Saleh and M. C. Teich, *Fundamentals of Photonics*, 2nd ed. Hoboken, NJ: Wiley, 2007.
[25] Y. Okamura, T. Negami, and S. Yamamoto, "Integrated optical isolator and circulator using nonreciprocal phase shifters: A proposal," *Appl. Opt.*, vol. 23, pp. 1886–1889, 1984.
[26] H. A. Haus, *Wave and Fields in Optoelectronics*. Englewood Cliffs, NJ: Prentice-Hall, 1984.

Zongfu Yu received the B.S. degree from the University of Science and Technology of China, Hefei, China, in 2004. He is currently working toward the Ph.D. degree in applied physics at Stanford University, Stanford, CA.

He has authored or coauthored more than ten refereed journal articles. His current research interests include silicon photonics, dynamic photonic structures, plasmonic devices, and computational electromagnetics.

Shanhui Fan (M'05–SM'06) received the Ph.D. degree in theoretical condensed matter physics from Massachusetts Institute of Technology (MIT), Cambridge, in 1997.

He was a Research Scientist at the Research Laboratory of Electronics at MIT prior to his appointment at Stanford. He is currently an Associate Professor of electrical engineering at Stanford University, Stanford, CA. He has authored or coauthored more than 160 refereed journal articles, has given over 120 invited talks, and holds 34 US patents. His current research interests include computational and theoretical studies of solid state and photonic structures and devices, especially photonic crystals, microcavities, and nanophotonic circuits and elements.

Dr. Fan is a Fellow of the Optical Society of America (OSA), a Fellow of the American Physical Society (APS), and a member of The International Society for Optical Engineers (SPIE). He received a National Science Foundation Career Award in 2002, a David and Lucile Packard Fellowship in Science and Engineering in 2003, the National Academy of Sciences Award for Initiative in Research in 2007, and the Adolph Lomb medal from the OSA in 2007.